Flux-Limited Nonequilibrium Electron Energy Transport in Warm Dense Gold

Z. Chen,[1] V. Sametoglu,[1] Y. Y. Tsui,[1,*] T. Ao,[2] and A. Ng[3,†]

[1]*Department of Electrical and Computer Engineering, University of Alberta, Edmonton, Alberta, Canada*
[2]*Sandia National Laboratories, Albuquerque, New Mexico, USA*
[3]*Department of Physics and Astronomy, University of British Columbia, Vancouver, British Columbia, Canada*

(Received 23 August 2011; published 16 April 2012)

An abrupt change in energy transport has been observed in femtosecond laser heated gold when the absorbed laser flux exceeds $\sim 7 \times 10^{12}$ W/cm^2. Below this value, the absorbed flux is carried by ballistic motion of nonthermal electrons produced in interband excitation. Above this value energy transport appears to include ballistic transport by nonthermal electrons and heat diffusion by thermalized hot electrons. The ballistic component is limited to a flux of $\sim 7 \times 10^{12}$ W/cm^2. This offers a unique benchmark for comparison with theory on nonequilibrium electron transport.

DOI: 10.1103/PhysRevLett.108.165001 PACS numbers: 52.50.Jm, 52.25.Fi, 52.25.Os, 52.38.−r

Electron energy transport is a basic process prevalent in broad disciplines. In plasma physics, much interest has been focused on heat transport across steep electron temperature gradients in laser-produced plasmas because of its vital role in direct-drive laser fusion [1]. This is a regime where the Spitzer-Harm theory [2] of diffusive heat flow breaks down. It has led to legislation of heat flux to be the minimum or harmonic mean of Spitzer-Harm flux and a free-streaming flux, with the latter reduced by a flux-limit factor f which is chosen in hydrodynamic simulations to replicate observations [3]. This *ad hoc* approach is followed by fully kinetic Fokker-Planck calculations [4–8]. Through comparison with Fokker-Planck results, a nonlocal heat flow formula has also been derived in a flux delocalized model for implementation in fluid codes [9,10]. While most earlier experiments in planar geometry have indicated f of $\sim$0.03, experiments in uniform spherical geometry point to f of $\sim$0.08 comparable to predictions of Fokker-Planck calculations [11].

In condensed matter physics on the other hand, much of the study on electron energy transport is related to ultrafast electron dynamics in fs-laser heated solids. Here, electrons are excited above the Fermi level creating a nonequilibrium distribution in the optical absorption region of the sample. At the surface of the heated solid, electrons with energy exceeding work function will start to escape. However, the process is rapidly limited by the space-charge field leading to the formation of an electron sheath. The number of escaped electrons is found to be small [12,13]. Inside the solid, energy transport is initially dominated by ballistic motion of nonthermal electrons moving at approximately Fermi speed [14–18] if the ballistic range exceeds optical absorption depth. As these excited electrons thermalize over a time scale of 0.5–1 ps [19–21], a Fermi distribution corresponding to an elevated electron temperature is established within the ballistic range. This distribution continues to drive diffusive heat flow into the sample, albeit at a lower speed.

Between plasma and condensed matter there is the so-called warm dense matter regime where the temperature of the state is comparable to Fermi energy and ions are strongly coupled [22]. Interest in warm dense matter is growing rapidly and a unique technique for producing such states is fs-laser excitation of solids based on isochoric and uniform heating of ultrathin metal foils [23]. The isochoric condition results from negligible lattice expansion and absence of melting during the heating pulse. Uniform heating is expected from ballistic transport of excited electrons as foil thickness is limited to less than the ballistic electron range. The technique has been used to obtain single-state ac conductivity and dielectric function data and to reveal nonequilibrium superheating in gold at high energy density [24–27]. However, ballistic electron transport has only been measured in the condensed matter regime at low laser flux [14–18]. Its behavior at high laser flux is unknown. This also underscores the critical lack of experimental data on electron energy transport in warm dense matter.

In this Letter we present the study of electron energy transport in gold heated by 400 nm, 45 fs laser pulses to energy densities $>10^{11}$ J/m^3. The focus on gold is dictated by its relevance to earlier measurements [14–18,24–27]. This is to help establish gold as a material standard for testing theory by broadening its scientific data base. Figure 1 shows schematic diagrams of our experiment

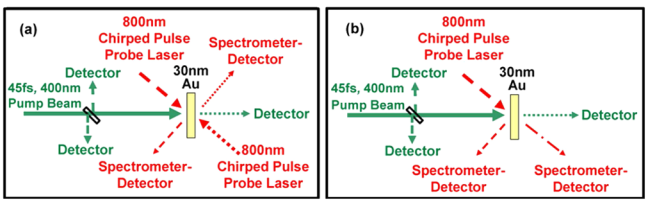

FIG. 1 (color online). Experimental setup for measurements of (a) front and rear side probe reflectivity and (b) front side probe reflectivity and transmissivity.

performed at the Advanced Laser Light Source in Varennes, Canada. The 400 nm pump and 800 nm probe beams are derived from an 800 nm main laser beam with time delays set by differences in optical path length. The pump beam is incident normally onto a freestanding, 30 nm-thick gold foil in vacuum, focused to a Gaussian spot of 62 μm diameter (FWHM). The prepulse intensity contrast at 800 nm is 10^{-6}, 10^{-5}, and 10^{-4} at, respectively, 10 ps, 1 ps and 0.5 ps before the peak of the pump pulse [28]. The corresponding contrast at 400 nm is expected to be about 10^{-12}, 10^{-10}, and 10^{-8}. Absorbed laser energy is determined from simultaneous measurements of the incident, reflected, and transmitted pulses with a spatial resolution of 5 μm. The probe beams are chirped to a duration of 6.5 ps (FWHM) to monitor temporal evolution in reflected or transmitted signals in a single shot, eliminating shot-to-shot irreproducibility. The probe beams are P polarized to enhance the sensitivity to ac conductivity of the heated state. They are focused to a spot diameter of 500 μm (FWHM). The reflected or transmitted probe light is imaged onto a spectrometer with an entrance slit viewing a region of 20 μm $\times$ 300 μm, centered with the pump focal spot on the corresponding foil surface. Absolute values of reflectivity and transmissivity are obtained using an *in situ* comparison of signals from heated and unheated regions of foil.

Our first measurement is the front and rear side probe reflectivity [Fig. 1(a)]. Figure 2 shows results for an absorbed laser flux Q_L of 5.9×10^{12} W/cm^2, corresponding to an excitation energy density of 4.5 MJ/kg. The recorded spectra contain spatial and temporal information. Spatial reflectivity profiles remain unchanged for more than 3 ps after laser excitation, indicating the absence of hydrodynamic expansion or lateral energy transport. To examine temporal behavior we use lineouts of reflectivity

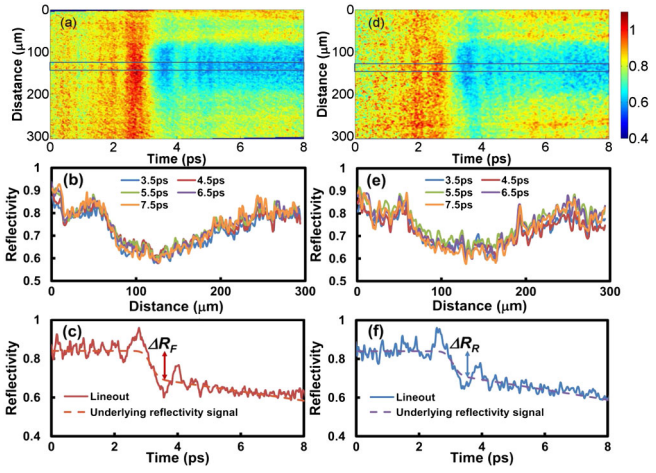

FIG. 2 (color online). Results of front (a)–(c) and rear (d)–(f) side probe reflectivity measurements for an absorbed laser flux of 5.9×10^{12} W/cm^2. Lineouts are taken from regions in spectra indicated by the rectangular boxes.

intensity from a 20 μm region at the center of the pump laser focal spot where laser intensity variation is $<10\%$. The rear side probe pulse arrives on target $\sim$120 fs after the front side probe. Good agreement is found between front and rear side reflectivity lineouts. This is consistent with uniform heating in the gold foil.

Aperiodic modulations are evident in reflectivity spectra and lineouts. However, these are not temporal variations in reflectivity since periods of their high frequency components are shorter than the $\sim$540 fs temporal resolution of the chirped pulse diagnostic [29]. They are traced to interference effects [30] caused by pump-induced optical Kerr effect [31] that produces cross phase modulation and spectral broadening [32] in the portion of the chirped pulse correlated with the pump pulse. Modulations with identical frequencies are also seen in reflectivity spectra measured from glass. Hence, the spectra are taken to be the superposition of interference and underlying reflectivity signals. The latter includes temporal segments before, during, and after laser excitation. Each of these is approximated by a linear fit to the lineout. The combined signal, convoluted with a Gaussian instrumental function of 540 fs FWHM, is depicted in Figs. 2(c) and 2(f).

The effect of absorbed laser flux on reflectivity is shown by the overlay of lineouts in Fig. 3. Shot-to-shot reproducibility in pump-probe delay is better than 100 fs, limited by alignment stability. No systematic difference in the onset of reflectivity change is seen between front and rear side observations. Lineouts shown have thus been shifted to overlap the rapid reflectivity changes during laser excitation. Interestingly, front and rear side lineouts remain in good agreement for Q_L up to 6.4×10^{12} W/cm^2, but at higher absorbed flux they differ substantially. Specifically, at the time marked by the dashed lines in the figure, change in the front side lineout increases with Q_L while the corresponding change in the rear side appears to be clamped at a nearly constant value. To quantify this unique feature we determine changes in front and rear side reflectivity at the end of laser excitation, ΔR_F and ΔR_R, using the underlying reflectivity signals as illustrated in Figs. 2(c) and 2(f). As seen in Fig. 4, the onset of

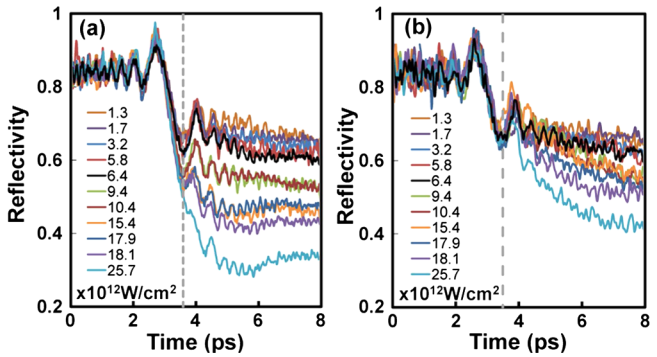

FIG. 3 (color online). Front (a) and rear (b) side probe reflectivity for different absorbed laser fluxes.

divergence between ΔR_F and ΔR_R is clearly evident above 6.4×10^{12} W/cm^2. Equally important, in such cases the rear side reflectivity shows a continuing decrease after laser excitation (Fig. 3). This suggests that two different energy transport processes are at play in determining rear side reflectivity as heating of the foil becomes nonuniform.

To understand these observations, we examine the pertinent processes. For a pump laser at 400 nm (3.1 eV), absorption depth in gold at normal conditions is 16 nm based on measured optical constants [33]. Laser absorption is dominated by the excitation of $5d$ electrons to the $6p$ band near the L point of the Brillouin zone since the threshold for the interband transition is 2.4 eV. The excited electrons initially fill unoccupied states up to 0.7 eV above Fermi energy. Some redistribution will rapidly follow by Auger decay and cascade. The thermalization time of electrons at 0.7 eV above Fermi energy is estimated to be 37 fs [34]. However, this is likely an underestimate. In an experiment on gold where electrons were excited by intraband absorption to states up to 1.84 eV above Fermi energy, electrons at 1 eV above Fermi energy were found to have a lifetime of ~600 fs [20]. Assuming a similar thermalization time in our experiment, initial transport will be dictated by laser-induced nonthermal electrons. As the foil thickness is much less than the 110 nm ballistic electron range [17], these electrons will make multiple transits through the foil aided by reflections at solid-vacuum interfaces [18], leading to uniform energy deposition. For a Fermi speed of $\sim 10^8$ cm/s [14–16,18], ballistic electron transit time in foil is ~30 fs. Uniform heating would be established in several transits long before the nonthermal electrons are thermalized. Accordingly, the observation of similar reflectivity on front and rear sides of the gold foil is attributed to uniform heating produced by ballistic transport of nonthermal electrons.

Laser absorption by plasmas is known to be dominated by collisionless absorption at laser flux $>10^{15}$ W/cm^2 and by inverse bremsstrahlung at lower flux [35]. The former process leads to the production of suprathermal electrons and heating of thin foils to high energy density has been attributed to refluxing of such electrons [36–39]. However, these absorption processes are not expected to play a significant role in our experiment where the heated foil remains in solid phase throughout the excitation laser pulse as evident from broadband dielectric function measurements and the persistence of interband transition at 400 nm [25].

Although we cannot equate reflectivity directly to electron temperature it is reasonable to surmise that a greater change in front side reflectivity signifies stronger heating near the front surface of foil. This can occur if absorbed laser flux Q_L exceeds the maximum energy flux Q_{NT} that can be transported by nonthermal electrons. Only the portion of Q_L equal to Q_{NT} will then be carried across the foil by ballistic transport while the excess flux becomes

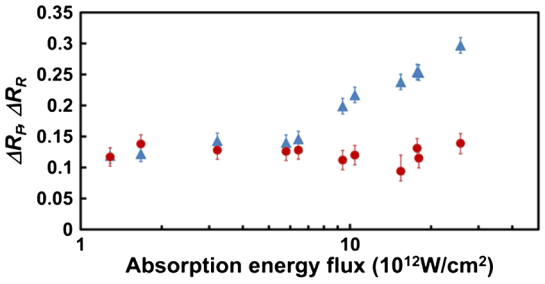

FIG. 4 (color online). Changes in front (triangles) and rear (circles) side reflectivity at the end of laser excitation as a function of absorbed laser flux.

localized in the laser absorption region, producing rapid heating at the front side of the foil. Subsequent transport of the excess flux will be driven primarily by heat diffusion as the electrons thermalize to form a Fermi distribution. This behavior can lead to a rear side reflectivity signal with $\Delta R_R < \Delta R_F$ at the end of the laser excitation (Fig. 4) followed by further decrease with time (Fig. 3).

In the absence of rigorous calculations, Q_{NT} is estimated using the product of nonthermal electron density n_{NT}, Fermi energy E_F, and Fermi speed v_F. We assume E_F to remain constant at 5.5 eV in the nonthermal system while noting that a shift in the Fermi level with electron temperature has been indicated in calculations [40]. We also adopt the observed v_F of 10^8 cm/s in gold [14–16,18] instead of the often quoted value of 1.4×10^8 cm/s. To determine n_{NT}, a second measurement is made using the simultaneous observation of reflectivity and transmissivity of a front side probe [Fig. 1(b)]. Results for $Q_L = 4.6 \times 10^{12}$ W/cm^2 are shown in Fig. 5 where the underlying reflectivity and transmissivity signals are again given by the method described above. Values of reflectivity R_F and transmissivity T_F at the end of laser excitation are used to derive ac conductivity from solutions of the Helmholtz equations for electromagnetic wave propagation in a uniform dielectric slab [24]. The results are presented in Fig. 6 as a function excitation energy density to allow direct comparison with earlier measurement using a pump laser pulse of 150 fs [24]. The small difference seen is attributed to the fact that our measurement yields conductivity at the end of laser excitation whereas the previous measurement is based on sampling over the

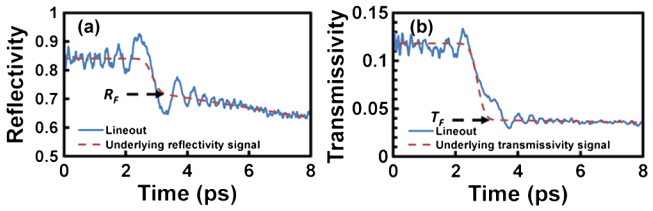

FIG. 5 (color online). Front side probe reflectivity and transmissivity for an absorbed laser flux of 4.6×10^{12} W/cm^2.

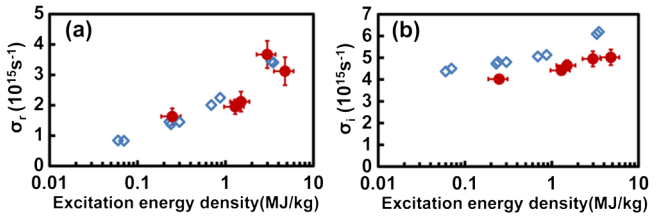

FIG. 6 (color online). Real and imaginary parts of ac conductivity as a function of excitation energy density: diamonds (our data), circles (data from Ref. [24]).

quasisteady state duration [24]. Since the dielectric function of warm dense gold is found to be Drude-like at 800 nm [25], our data are used in the Drude model to derive conduction electron density n_e. The result is presented in Fig. 7(a). Here we make a final assumption of equating n_{NT} to n_e in the calculation of Q_{NT}, drawing upon the parallel between thermal and electrical conduction. As suggested by linear extrapolation of the data in Fig. 7(b), Q_L/Q_{NT} increases to unity when Q_L reaches $\sim 7 \times 10^{12}$ W/cm^2. This coincidence with the onset of divergence between front and rear side reflectivity leads to our assertion of flux-limited ballistic transport at play. However, that the flux limit is equal to the nonthermal electron energy flux as calculated may just be fortuitous. The latter needs to be determined from more rigorous models.

The above phenomenology also predicts a flux limit that changes with Q_{NT} when Q_L is increased. This may appear inconsistent with ΔR_R being clamped at a fixed value when $Q_L > \sim 7 \times 10^{12}$ W/cm^2 (Fig. 4). Such a saturation effect is likely the result of the transition of ballistic to diffusive energy transport. Once the flux limit is first reached during the pump laser pulse, additional absorbed flux will begin to be localized in the absorption layer at the front surface of the foil since conduction electron density produced by interband excitation increases relatively slowly with absorbed flux [Fig. 7(a)]. This leads to enhanced heating of the front surface of the foil causing front side reflectivity to continue to decrease. At the same time, additional decrease in rear side reflectivity is delayed until thermalization of nonthermal electrons has produced a significant diffusive heat flux towards the foil rear surface. The interplay between thermalization and transport under such conditions is also not known. We need to understand how

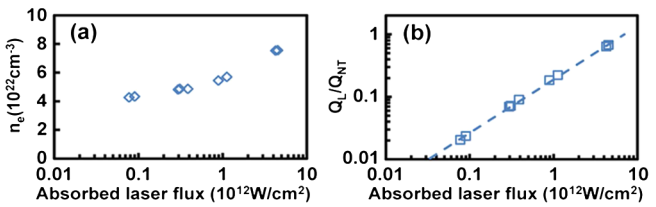

FIG. 7 (color online). Conduction electron density and Q_L/Q_{NT} as a function of absorbed laser flux.

nonequilibrium electron distribution may affect electron collisions which in turn modify the electron distribution, and how this may regulate electron energy transport.

As noted above electrons can escape from the heated foil by photoemission. However, this cannot account for significant reduction in energy transport in our experiment. In a recent study on silver heated with 0.2 mJ, 70 fs, 800 nm laser pulse at an incident flux of 1.5×10^{14} W/cm^2, 8×10^7 electrons were estimated to have escaped from the target with an average velocity of 1.2×10^9 cm/s [13]. These electrons carry away 5.4 nJ of energy or a heat flux of $\sim 4 \times 10^9$ W/cm^2 if they were to originate from the same area as the pump laser spot and in the same duration as the pump laser pulse. Even less energy loss would be expected in our experiment where the incident pump laser flux is $< 6 \times 10^{13}$ W/cm^2. Energy loss may also occur via lateral transport of escaped electrons onto the target surface outside the heated spot causing heating and reflectivity change in the affected area. However, our measured probe spatial reflectivity profiles reveal no significant heating outside the pump laser spot even for the absorbed laser flux of 2.6×10^{13} W/cm^2.

In conclusion, measurements of front and rear side reflectivity of fs-laser heated gold foils have revealed an abrupt change in energy transport when the absorbed energy flux exceeds $\sim 7 \times 10^{12}$ W/cm^2, corresponding to an excitation energy density of $\sim 10^{11}$ J/m^3. Below this value, the absorbed flux is carried by the ballistic motion of nonthermal electrons produced by laser-induced interband excitation. Above this value, the flow of absorbed energy appears to include ballistic transport by nonthermal electrons and heat diffusion by thermalized hot electrons, with the ballistic flux being limited to $\sim 7 \times 10^{12}$ W/cm^2. This offers a unique benchmark for comparison with theory on nonequilibrium electron transport. It also sets a limit on uniform energy deposition that can be achieved in the isochoric heating of gold by femtosecond lasers.

This work is supported by the Natural Sciences & Engineering Research Council of Canada and the Canadian Institute for Photonic Innovations. We also wish to thank Advanced Laser Light Source for the use of the laser facility and technical support, and M. W. C. Dharma-Wardana for valuable discussions.

*Corresponding author.
tsui@ece.ualberta.ca
†Corresponding author.
nga@physics.ubc.ca

[1] J. Nuckolls, L. Wood, A. Thiessen, and G. Zimmerman, Nature (London) **239**, 139 (1972).
[2] L. Spitzer and R. Harm, Phys. Rev. **89**, 977 (1953).
[3] R. C. Malone, R. L. McCrory, and R. L. Morse, Phys. Rev. Lett. **34**, 721 (1975).
[4] A. R. Bell, R. G. Evans, and D. J. Nicholas, Phys. Rev. Lett. **46**, 243 (1981).

[5] R. J. Mason, Phys. Rev. Lett. **47**, 652 (1981).
[6] J. P. Matte and J. Virmont, Phys. Rev. Lett. **49**, 1936 (1982).
[7] J. R. Albritton, Phys. Rev. Lett. **50**, 2078 (1983).
[8] J. P. Matte, T. W. Johnston, J. Delettrez, and R. L. McCrory, Phys. Rev. Lett. **53**, 1461 (1984).
[9] J. F. Luciani, P. Mora, and J. Virmont, Phys. Rev. Lett. **51**, 1664 (1983).
[10] J. F. Luciani, P. Mora, and R. Pellat, Phys. Fluids **28**, 835 (1985).
[11] J. Delettrez, Can. J. Phys. **64**, 932 (1986), and references therein.
[12] H. Park and J. M. Zuo, Appl. Phys. Lett. **94**, 251103 (2009).
[13] P. Zhu *et al.*, Appl. Phys. Lett. **97**, 211501 (2010).
[14] S. D. Brorson, J. G. Fujimoto, and E. P. Ippen, Phys. Rev. Lett. **59**, 1962 (1987).
[15] T. Juhasz, H. E. Elsayed-Ali, G. O. Smith, C. Suarez, and W. E. Bron, Phys. Rev. B **48**, 15488 (1993).
[16] C. Suarez, W. E. Bron, and T. Juhasz, Phys. Rev. Lett. **75**, 4536 (1995).
[17] J. Hohlfeld, J. G. Müller, S.-S. Wellershoff, and E. Matthias, Appl. Phys. B **64**, 387 (1997).
[18] X. Liu, R. Stock, and W. Rudolph, Phys. Rev. B **72**, 195431 (2005).
[19] W. S. Fann, R. Storz, H. W. K. Tom, and J. Bokor, Phys. Rev. Lett. **68**, 2834 (1992).
[20] W. S. Fann, R. Storz, H. W. K. Tom, and J. Bokor, Phys. Rev. B **46**, 13592 (1992).
[21] C.-K. Sun, F. Vallee, L. Acioli, E. P. Ippen, and J. G. Fujimoto, Phys. Rev. B **48**, 12365 (1993).
[22] A. Ng, T. Ao, F. Perrot, M. W. C. Dharma-Wardana, and M. E. Foord, Laser Part. Beams **23**, 527 (2005).
[23] A. Forsman, A. Ng, G. Chiu, and R. M. More, Phys. Rev. E **58**, R1248 (1998).
[24] K. Widmann, T. Ao, M. E. Foord, D. F. Price, A. D. Ellis, P. T. Springer, and A. Ng, Phys. Rev. Lett. **92**, 125002 (2004).
[25] Y. Ping, D. Hanson, I. Koslow, T. Ogitsu, D. Prendergast, E. Schwegler, G. Collins, and A. Ng, Phys. Rev. Lett. **96**, 255003 (2006).
[26] T. Ao, Y. Ping, K. Widmann, D. F. Price, E. Lee, H. Tam, P. T. Springer, and A. Ng, Phys. Rev. Lett. **96**, 055001 (2006).
[27] R. Ernstorfer, M. Harb, C. T. Hebeisen, G. Sciaini, T. Dartigalongue, and R. J. Dwayne Miller, Science **323**, 1033 (2009).
[28] C. A. Popovici, R. A. Ganeev, F. Vidal, and T. Ozaki, in Advanced Annual Report 2007–2008, (2008), p. 48 lmn.emt.inrs.ca/EN/ALLS_Pub.htm.
[29] J.-P. Geindre, P. Audebert, S. Rebibo, and J.-C. Gauthier, Opt. Lett. **26**, 1612 (2001).
[30] E. Tokunaga, A. Terasakiy, and T. Kobayashi, J. Opt. Soc. Am. B **12**, 753 (1995).
[31] F. Hache, D. Ricard, C. Flytzanis, and U. Kreibig, Appl. Phys. A **47**, 347 (1988).
[32] K. Y. Kim, I. Alexeev, and H. M. Milchberg Appl. Phys. Lett. **81**, 4124 (2002).
[33] P. B. Johnson and R. W. Christy, Phys. Rev. B **6**, 4370 (1972).
[34] D. Pine and P. Nozieres, *The Theory of Quantum Liquids* (Benjamin, New York, 1966).
[35] P. Gibbon and E. Förster, Plasma Phys. Controlled Fusion **38**, 769 (1996).
[36] G. Gregori *et al.*, Contrib. Plasma Phys. **45**, 284 (2005).
[37] S. D. Baton *et al.*, High Energy Density Phys. **3**, 358 (2007).
[38] P. Neumayer, H. J. Lee, D. Offerman, E. Shipton, A. Kemp, A. L. Kritcher, T. Döppner, C. A. Back, and S. H. Glenzer, High Energy Density Phys. **5**, 244 (2009).
[39] P. M. Nilson *et al.*, Phys. Rev. Lett. **105**, 235001 (2010).
[40] V. Recoules, J. Clerouin, G. Zerah, P. M. Anglade, and S. Mazevet, Phys. Rev. Lett. **96**, 055503 (2006).